HIGH-FIDELITY VISCOUS ANALYSIS OF MAV WING NONLINEAR AEROELASTIC INTERACTION WITH NON-UNIFORM UNSTEADY FLOW

Vladimir V. Golubev, golubd1b@erau.edu
Reda R. Mankbadi, mankbadr@erau.edu
Florida Center for Advanced Aero Propulsion, Computational Aero Propulsion Group
Embry-Riddle Aeronautical University, Daytona Beach, FL 32114, USA

Abstract. *The work develops a high-accuracy viscous analysis of nonlinear aeroelastic interaction of a Micro Air Vehicle's (MAV) wing section with a non-uniform, unsteady upstream flow. In the implemented iterative procedure, a set of governing Navier-Stokes equations is solved simultaneously with nonlinear equations of motion of the structure, so that the fluid and structure are treated as a coupled dynamic system. The numerical procedure employs a high-order low-pass filter operator which selectively damps the poorly resolved high-frequency content to retain numerical accuracy and stability over a wide range of flow regimes. An efficient analytical model is used to introduce an unsteady incompressible 2D vortical flow perturbation inside the computational domain through a source term in the momentum equations. Strongly coupled, nonlinear unsteady aerodynamic and structural responses of an elastically-mounted, rigid airfoil subject to a viscous upstream flow with imposed harmonic, high-amplitude vortical gust are examined in a test study, with focus on the wing section transition to limit cycle oscillations (LCO).*
Keywords: *MAV, CFD, Gust, Aeroelastic, LCO*

1. INTRODUCTION

The current study is motivated by the need to develop an accurate, robust prediction tool for analysis of nonlinear aeroelastic responses of an aircraft wing to high-intensity upstream flow turbulence. Such a tool should be able to accurately account for both structural and aerodynamic nonlinearities in aeroelastic systems that could lead, e.g., to a premature transition to flutter and/or LCO of the structure. A high-fidelity analysis is crucial for light-weight MAVs particularly sensitive to the upstream flow disturbances (gusts) whose impact may compromise the MAV flight stability and performance. On the other hand, by using a robust analysis tool, a smart flexible wing structure may actually be designed to alleviate the severity of the gust impact, a fixture so wide-spread in natural flyers (Shyy et al, 2008). In this paper, we addresses the development of such a unified prediction tool on the basis of a high-accuracy Navier-Stokes solver (Visbal and Gaitonde, 2002) that has been successfully applied to a variety of steady and unsteady flow problems.

We start with reviewing the implemented numerical model and emphasize the Implicit Large Eddy Simulation (ILES) capability (Visbal et al, 2003) based on combining high-order compact schemes with Pade-type low-pass filtering procedure to ensure stability. The method is particularly attractive for current applications due to its ability to seamlessly handle mixed laminar, transitional and turbulent flows.

We then discuss an efficient 2-DOF structural response module integrated with the Navier-Stokes solver for conducting a high-fidelity viscous, nonlinear study of gust interaction with a flexible wing section. Here, we introduce a 2D gust source model imposing a vortical, incompressible unsteady flow perturbation inside the computational domain through a source term in the flow solver's momentum equations.

Finally, we examine results of the viscous analysis of coupled aerodynamic and aeroelastic responses of the symmetrical Joukowski airfoil to a high-amplitude impinging gust. Moderate-Reynolds number simulations are conducted for a range of flow velocities between 15 and 19 m/s crossing the flutter boundary with the set of structural parameters corresponding to the experimental data of Berggren (2004). This investigation reveals the gust effect on the airfoil transition to LCO and provides illustration of highly complex unsteady, nonlinear, viscous fluid-structure interaction phenomena and characteristic airfoil surface pressure fluctuations resulting from multiple structural excitation frequencies. The study thus paves the way to future detailed parametric studies elucidating the effect of gust frequency, amplitude and overall configuration on the coupled unsteady aerodynamic and aeroelastic responses, which could lead, e.g., to optimization of structural parameters in order to minimize the impact of upstream flow disturbances on the MAV wing aerodynamic performance and flight stability.

2. NUMERICAL FLOW SOLUTION

The employed high-accuracy numerical code solves a set of the compressible Navier-Stokes equations (Eq. 1) represented in the conservative, time-dependent form in the generalized curvilinear computational coordinates (ξ,η,ζ,τ) transformed from the physical coordinates (x,y,z,t):

$$\frac{\partial}{\partial \tau}(\frac{\vec{Q}}{J}) + \frac{\partial \vec{F}_i}{\partial \xi} + \frac{\partial \vec{G}_i}{\partial \eta} + \frac{\partial \vec{H}_i}{\partial \zeta} + \frac{1}{\mathrm{Re}}[\frac{\partial \vec{F}_v}{\partial \xi} + \frac{\partial \vec{G}_v}{\partial \eta} + \frac{\partial \vec{H}_v}{\partial \zeta}] = \vec{S} \tag{1}$$

The solution vector $\vec{Q} = (\rho, \rho u, \rho v, \rho w, \rho e)$ is defined in terms of the flow density ρ, Cartesian flow velocity components (u, v, w), and flow specific energy,

$$e = \frac{T}{\gamma(\gamma - 1)M_\infty^2} + \frac{1}{2}(u^2 + v^2 + w^2),$$

with perfect gas relationship $p = \rho T / \gamma M_\infty^2$ connecting the flow pressure p, temperature T, and the freestream Mach number M_∞ (γ is the specific heat ratio). The other variables in Eq. (1) include the inviscid flux vectors defined by,

$$\vec{F}_i = \begin{bmatrix} \rho\hat{u} \\ \rho u\hat{u} + \hat{\xi}_x p \\ \rho v\hat{u} + \hat{\xi}_y p \\ \rho w\hat{u} + \hat{\xi}_z p \\ (\rho e + p)\hat{u} - \hat{\xi}_t p \end{bmatrix}, \quad \vec{G}_i = \begin{bmatrix} \rho\hat{v} \\ \rho u\hat{v} + \hat{\eta}_x p \\ \rho v\hat{v} + \hat{\eta}_y p \\ \rho w\hat{v} + \hat{\eta}_z p \\ (\rho e + p)\hat{v} - \hat{\eta}_t p \end{bmatrix}, \quad \vec{H}_i = \begin{bmatrix} \rho\hat{w} \\ \rho u\hat{w} + \hat{\zeta}_x p \\ \rho v\hat{w} + \hat{\zeta}_y p \\ \rho w\hat{w} + \hat{\zeta}_z p \\ (\rho e + p)\hat{w} - \hat{\zeta}_t p \end{bmatrix}, \tag{2}$$

the transformation Jacobian, $J = \partial(\xi, \eta, \zeta, \tau) / \partial(x, y, z, t)$, the metric quantities defined, e.g., as $\hat{\xi}_x = (J^{-1})\partial\xi / \partial x$, etc., and the transformed flow velocity components,

$$\begin{aligned} \hat{u} &= \hat{\xi}_t + \hat{\xi}_x u + \hat{\xi}_y v + \hat{\xi}_z w \\ \hat{v} &= \hat{\eta}_t + \hat{\eta}_x u + \hat{\eta}_y v + \hat{\eta}_z w \\ \hat{w} &= \hat{\zeta}_t + \hat{\zeta}_x u + \hat{\zeta}_y v + \hat{\zeta}_z w \end{aligned} \tag{3}$$

The viscous flux vectors, $\vec{F}_v$, $\vec{G}_v$ and $\vec{H}_v$, are defined, e.g., in Anderson et al (1984), while $\vec{S}$ represents the source term which in the current work generates an incompressible unsteady vortical perturbation upstream of the wing section. All flow variables are normalized by their respective reference freestream values except for pressure which is nondimensionalized by $\rho_\infty u_\infty^2$.

Note that the governing equations are represented in the original unfiltered form used unchanged in laminar, transitional or fully turbulent regions of the flow, with Visbal et al (2003) providing further details on the code's employed Implicit LES (ILES) procedure in which a high-order low-pass filter operator is applied to the dependent variables during the solution process, in contrast to the standard LES addition of sub-grid stress (SGS) and heat flux terms. The resulting filter selectively damps the evolving poorly resolved high-frequency content of the solution.

The code employs a finite-difference approach to discretize the governing equations, with all the spatial derivatives obtained using the high-order compact-differencing schemes from Lele (1992). For the wing section computations of the current paper, a sixth-order scheme is used. At boundary points, higher-order one-sided formulas are utilized which retain the tridiagonal form of the scheme. In order to ensure that the Geometric Conservation Law (GCL) is satisfied, the time metric terms are evaluated employing the procedures described in detail in Visbal and Gaitonde (2002). Finally, the time marching is accomplished by incorporating a second-order iterative, implicit approximately-factored procedure as described in Visbal et al (2003).

3. STRUCTURAL RESPONSE MODELS

The current work develops and implements an aeroelastic response module within the structure of the viscous flow solver. The modified code thus acquires the capability to conduct fully coupled nonlinear aeroelastic, aerodynamic and aeroacoustic analyses of structure's unsteady responses. In the employed formulation, the equations governing the fluid motion are essentially coupled with equations governing the 2-DOF airfoil motion, so that the fluid and structure are treated as a single dynamic system.

The general form of a rigid airfoil's 2-DOF motion may be derived by using Lagrange's equations and considering the total energy of motion for the wing section's center of mass. This approach leads to a set of nonlinear equations of

motion for the airfoil plunging and pitching amplitudes *y=h(t)* and *α(t)*, respectively (see Fig. 1). The current work employs a form of nonlinear equations from O'Neil and Strganac (1998) which can be reduced to the following classical quasilinear form with the assumptions of small-amplitude oscillations and negligible gravity effects:

$$M_s\ddot{v} + C_s\dot{v} + K_s v + F(v) = \big(-L(t), M(t)\big), \tag{4}$$

where $\boldsymbol{v}(t)=[h(t),\ \alpha(t)]$ is the displacement vector, and *L(t)* and *M(t)* are the lift and pitching moment about the rotation axis, correspondingly.

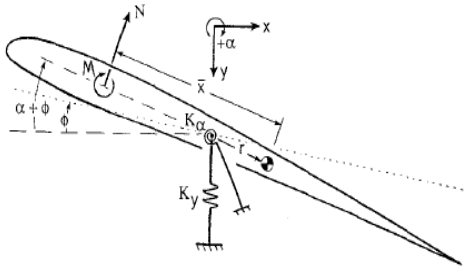

Figure 1. 2-DOF rigid airfoil aeroelastic model

In Eq. (4), the structural wing section properties include the linear mass matrix $\boldsymbol{M_s}$ and the damping matrix $\boldsymbol{C_s}$, given by

$$M_s = \begin{bmatrix} mass & S_\alpha \\ S_\alpha & I_\alpha \end{bmatrix}, \quad C_s = 2\cdot\begin{bmatrix} \zeta_h\sqrt{k_h\cdot mass} & 0 \\ 0 & \zeta_\alpha\sqrt{k_\alpha\cdot I_\alpha} \end{bmatrix}, \tag{5}$$

where *mass* denotes the mass of the wing section, I_α is the mass moment of inertia, S_α is the static moment, and ζ_h and ζ_α represent the damping logarithmic decrements. In the current problem, the nonlinearity is introduced in the aeroelastic system through the nonlinear stiffness function $\boldsymbol{F}$ taken in the form,

$$F(v) = \big(k_h h(t), k_{\alpha 1}\alpha(t) + k_{a3}\alpha^3(t)\big), \tag{6}$$

where k_h, $k_{\alpha 1}$ and $k_{\alpha 3}$ are the spring constants.

To validate the aeroelastic response module, and to investigate the airfoil response near the flutter boundary, we first examine solutions of Eq. (4) obtained for the flat plate, with the unsteady aerodynamic forces on the right hand side of Eq. (4) defined analytically in Bisplinghoff et al (1957). The following structural parameters are considered, originally imposed in the experimental study of Berggren (2004) for a NACA-0010 wing section (with the airfoil chord of 0.22m and the pitching center displaced by 0.0024m from the midchord towards the leading edge):

$$\begin{aligned} &mass = 2.55(kg) \\ &S_\alpha = 0.00104(kg\cdot m), I_\alpha = 0.00252(kg\cdot m^2) \\ &\zeta_h = 0.0055, \zeta_\alpha = 0.018 \\ &k_h = 450(N/m), k_{\alpha 1} = 9.3(N/m), k_{\alpha 3} = 55(N/m) \end{aligned} \tag{7}$$

The airfoil is initially excited with the plunging and pitching perturbations corresponding to $|\dot{h}| = 0.002$ and $|\dot{\alpha}| = 0.005$. Fig. 2 shows comparison of our results with analogous numerical predictions and experimental data from Berggren (2004). The figure exhibits the established LCO amplitudes for the airfoil's angle of attack (AOA=α) and vertical displacement (*h*) oscillations, respectively. For each flow velocity in the displayed range, the results are produced by integrating Eq. (4) for a sufficient period of time using the 5th order explicit Runge-Kutta method, until the amplitude variations do not exceed a tolerance value. The onset of LCO corresponds to reaching the critical (flutter) speed beyond which the exponential growth of the airfoil oscillations is precluded due to the non-zero nonlinear term spring constant $k_{\alpha 3}$. Note that both numerical flat plate calculations shown in Figure 2 match closely and predict the flutter speed around 16m/s. A significant discrepancy from the experimental data for the plunging amplitude is extensively discussed in Berggren (2004).

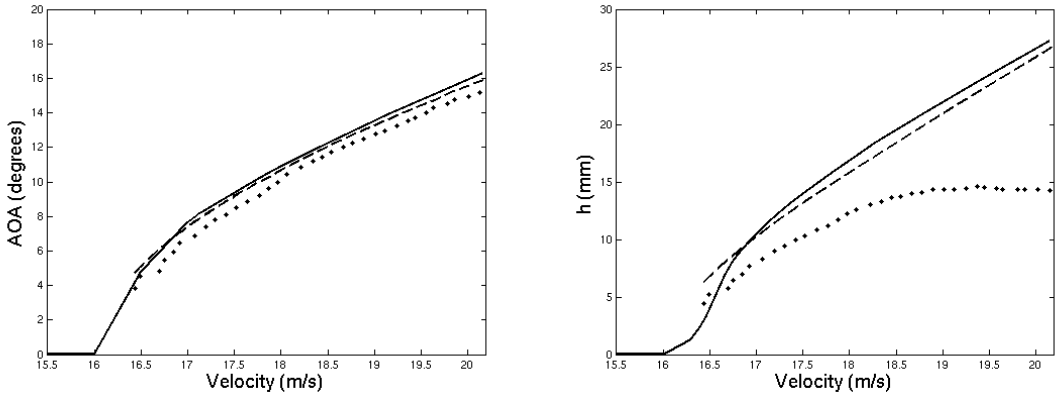

Figure 2. Pitching (left) and plunging (right) flat plate LCO amplitudes: current aeroelastic model predictions (solid line), numerical analysis (dashed line) and experiment (markers) from Berggren (2004)

The current study integrates the nonlinear aeroelastic response module with the flow solver. With aerodynamic loads in Eq. (4) supplied through Navier-Stokes simulations, the structural response system reduces to a set of first-order differential equations. In the code's time marching procedure, the implemented aeroelastic response module thus determines the displacement vector which, in turn, defines the grid motion. In addition, at each physical time step, an internal iterative loop is required to achieve the balance of the new airfoil position and the corresponding unsteady flowfield. This loop is merged with the subiterative procedure implemented as part of the flow solver's implicit time marching scheme.

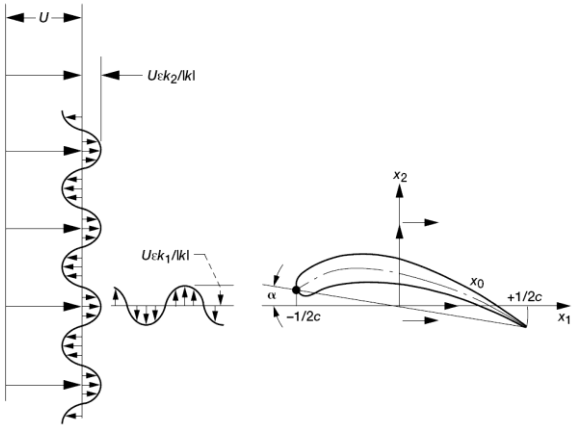

Figure 3. Gust-airfoil interaction problem

4. GUST SOURCE MODEL

In this study, we examine a nonlinear response of a flexible airfoil to an impinging unsteady, vortical perturbation imposed far upstream of the airfoil on the steady-state uniform mean flow. In general, the velocity field of such perturbation, representing, e.g., a turbulent flow fluctuation, may be described in terms of the following Fourier spectrum containing various perturbation frequencies and wave numbers,

$$u'(\vec{x},t) = \mathrm{Re}\{\int_{\omega}\sum_{\vec{k}} A_{\vec{k}}(\vec{x})\exp[i(\vec{k}\cdot\vec{x}-\omega t)]\} \tag{8}$$

For numerical simulations of unsteady flow interaction with an airfoil, a single two-dimensional vortical perturbation velocity harmonic (gust) is selected in the form,

$$\begin{aligned} u_g &= \varepsilon_u \cos(\alpha x + \beta y - \omega_g t) \\ v_g &= \varepsilon_v \cos(\alpha x + \beta y - \omega_g t) \end{aligned}, \tag{9}$$

with the gust amplitudes,

$$\varepsilon_u = -\left(\frac{\varepsilon_g \beta u_\infty}{\sqrt{\alpha^2+\beta^2}}\right), \qquad \varepsilon_v = \left(\frac{\varepsilon_g \alpha u_\infty}{\sqrt{\alpha^2+\beta^2}}\right), \tag{10}$$

where ε_g is the gust intensity relative to the mean flow, α and β are the gust wave numbers in the x and y directions, ω_g is the imposed gust frequency, and u_∞ is the convective freestream velocity. Note that $\alpha = \omega_g / u_\infty$ and $\beta = \alpha \tan\chi$, where χ is the angle between the normal vector of the gust phase front and the x-axis.

The approach implemented here to generate a 2D gust inside a computational domain extends the analysis of Lockard and Morris (1998) where an analytical 1D gust source model was developed. Details of the present derivations are included in Golubev et al (2009) where we show that in order to generate the gust of the form in Eq. (9) downstream of the source region $|x - x_s| \le \pi / b$, one should impose the following source components in the flow momentum equations,

$$\begin{aligned} s_u(x,y,t) &= \beta K g(x)\lambda(y)\cos(\omega_g t - \beta y - \alpha x_s) \\ s_v(x,y,t) &= K g'(x)\lambda(y)\sin(\omega_g t - \beta y - \alpha x_s) \end{aligned}, \tag{11}$$

where the exact expressions for the functions $g(x)$, $\lambda(y)$ and constant K can be found in Golubev et al (2009). The main benefit of the current approach is that in contrast to standard procedures used, e.g., in Golubev et al (2005), the proposed method avoids the difficulty of imposing the proper vortical flow disturbance at the upstream boundary, and thus allows stretched computational grids throughout the farfield to minimize spurious boundary reflections.

To verify the gust source model, results are obtained for the unsteady viscous flow simulations around stationary and pitching SD7003 airfoil section in the laminar flow regime with M_∞ =0.1 and $\mathrm{Re} = \rho u_\infty c / \mu = 10{,}000$, where c is the airfoil chord. The airfoil pitching motion is prescribed in terms of the harmonic variation of the airfoil angle of attack with frequency ω_{pt} relative to the pitching center x_p, $\alpha(t) = \alpha_m \sin\omega_{pt} t + \alpha_0$. Computations are performed with the following parameters of the pitching motion: $\alpha_0 = 0^0$, $\alpha_m = 21.5^0$, $\omega_{pt} = 8$, $x_p = 0.25c$.

The results are presented for a 2D gust with intensity ε_g =0.1 convecting with $\chi = 45^0$ and oscillating with reduced frequency $k_g = \omega_g c / 2u_\infty = 2$. Note that with the code's non-dimensionalization, the gust wavenumbers and frequency are $\alpha = \beta = \omega_g = 2k_g = 4$. A fixed non-dimensional time step of $\Delta t = 5\times10^{-5}$ is chosen, which corresponds to the Courant number close to 10. All variables in the figures below are presented in the non-dimensional form unless specified otherwise.

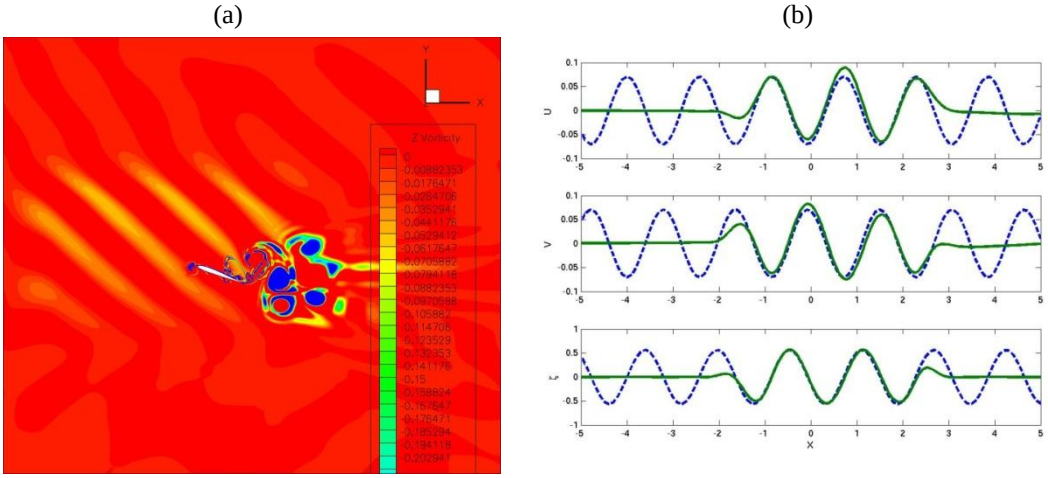

Figure 4. (a) Contour plot for flow vorticity at *t=5.6*, with x_s=*-3.5*, (b) Flow velocity and vorticity along the line *y=1* at *t=6*, with x_s=*-1.5*

Fig. 4(a) shows a time snapshot of the contour plot for the flow vorticity $\varpi_z = \partial v/\partial x - \partial u/\partial y$ obtained at t=5.6. The gust is generated using the momentum source components (11) in a region specified by x_s=-3.5 and b=5 in Eq. (11). Note the vortical patterns generated by the gust and the pitching airfoil. Since the grid is significantly stretched in the selected gust source region, the generated gust amplitude appears to be distributed non-uniformly in y-direction.

Another set of results was produced with x_s=-1.5. Fig. 4(b) shows the comparison of the analytical and numerical predictions for the flow velocity components *u*, *v* and vorticity ϖ_z at *t*=6, obtained along the convection line *y*=1. Note that the computed velocities (solid lines) deviate from the analytical predictions due to the impact of the potential pressure waves propagating from the airfoil. However, the vorticity plots match very well. This gust source region is used in all subsequent studies.

5. RESULTS AND DISCUSSION

Numerical simulations of the aeroelastic airfoil response to the impinging gust are performed for flow configurations with V=15-19m/s and Re=50,000. Note that, in general, the LCO onset, transition and resulting oscillation amplitudes and frequency may be sensitive to the character of either short-term (initial) or continuous (gust) unsteady forcing, but such discussion is beyond the scope of the present work.

The results presented below are obtained from the code parallel simulations with 3D mesh efficiently partitioned into a set of 32 overlapped blocks assigned to different processors. The baseline 649 × 395 × 3 grid is generated around a symmetric, 12%-thick Joukowski airfoil, with carefully rounded trailing edge to avoid any numerical instability. We consider the unsteady viscous response of the flexible Joukowski airfoil to the impinging 2D gust generated in the upstream source region with k_g =1 (ω_g =2) and ε_g =0.1. A fixed time step of $\Delta t \approx 10^{-4}$ is used in all simulations carried out for 3×10^6 time steps to let the structure establish its long-term response, with each case taking about 2 weeks of CPU time to complete. The cases involving transition to LCO typically take more time because of the larger number of subiterations required in the aeroelastic module to mutually adjust the airfoil position with a new unsteady flow condition. In addition to recording the complete time histories of structural and aerodynamic characteristics, a detailed frequency content of the mean, RMS and higher harmonics of the established airfoil unsteady response is obtained for the base frequency of ω=0.125, and resolved up to ω=8 by taking 128 records of the solution time history during its last time period of $\Delta t \approx 50$.

For simulations of the flow around a 1-DOF pitching symmetrical Joukowski airfoil, we consider the set of structural parameters in Eq. (7). Note that the previous flat-plate analysis for such structural characteristics established the flutter boundary around 16 m/s. Thus, we first present results obtained for the mean flow velocities V=15m/s and 18m/s that correspond to the pre-flutter and post-flutter flow conditions according to the simplified flat-plate analysis.

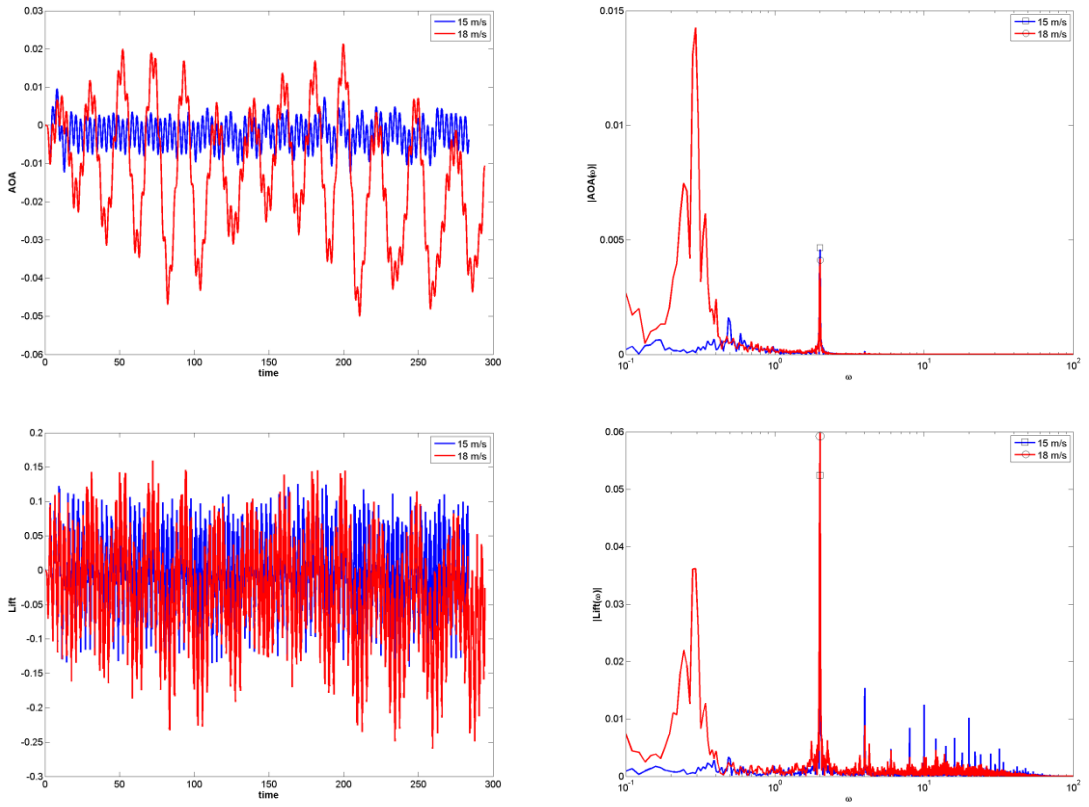

Figure 5. Time histories and FFT spectra for airfoil gust response at 15 and 18m/s, quasilinear structural model

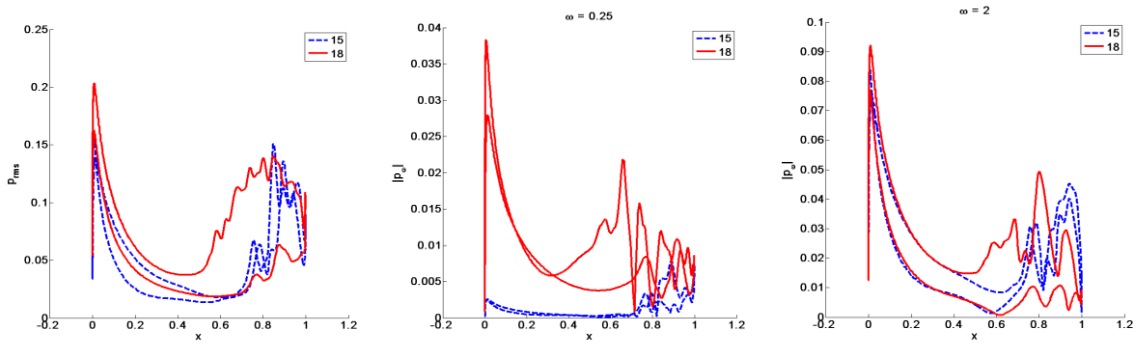

Figure 6. RMS and FFT harmonics of unsteady surface pressure for airfoil gust response at 15 and 18m/s, quasilinear structural model

Fig. 5 provides the comparison of time histories and corresponding FFT frequency spectra for the airfoil angle of attack and unsteady lift fluctuations. The gust imposes a continuous forced excitation of the structure which responds with oscillations at the gust frequency, but the results also indicate a clear contrast between responses for the two flow velocities, with the case of 18m/s showing a distinct superposition of the gust and LCO frequencies ($\omega_{LCO} \sim 0.3$) and the latter practically subdued in the case of 15m/s. A rather wide peak at the LCO frequency is attributed to the transitional airfoil behavior characterized by frequency shifts towards establishing the long-term structural response. Interestingly, the aerodynamic characteristics are still dominated by the gust response and appear similar in both cases, while the structural response clearly shows the difference between the two cases. Note that the amplitude of the structural LCO response and its effect on the airfoil aerodynamic performance will significantly increase for larger flow velocities. In the present study, the maximum amplitudes of structural oscillations do not exceed 3^0 for pitching and 4% of chord for plunging oscillations, for which the quasilinear form of equations of motion in Eq. (4) is adequate.

Fig. 6 compares RMS and FFT harmonics of the unsteady surface pressure. The frequency harmonics corresponding to the LCO (approximately) and gust frequencies are obtained based on 128 records of the established long-term airfoil response. Note that at 15m/s, the unsteady response is almost entirely determined by the gust impact, while above the flutter boundary, the effect of the structural motion becomes significant. In both cases, the unsteady surface pressure fluctuations are evident close to the airfoil trailing edge.

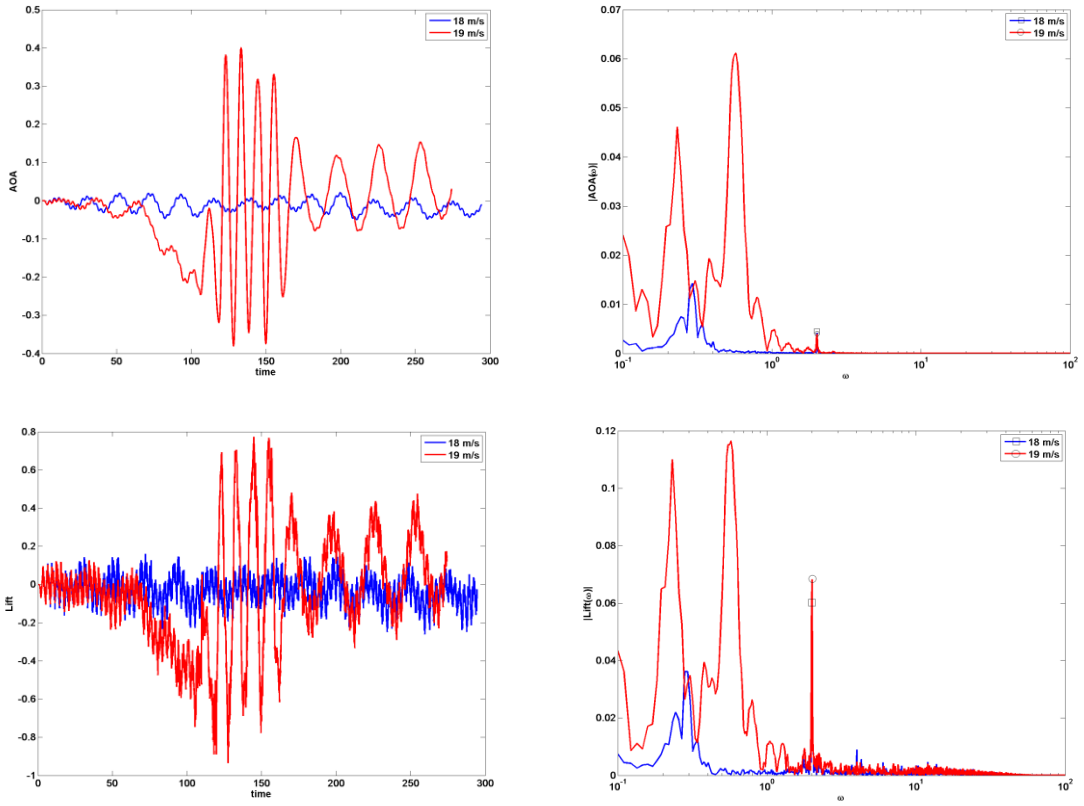

Figure 7. Time histories and FFT spectra for airfoil gust response at 18 and 19m/s, quasilinear structural model

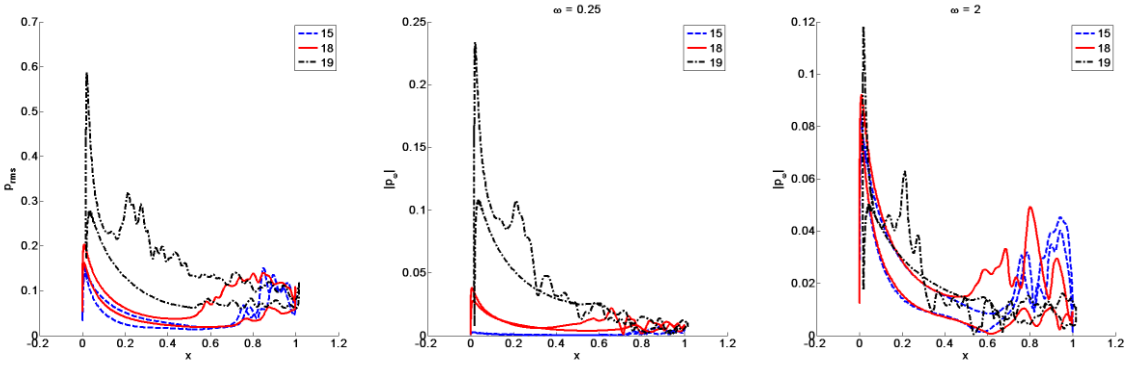

Figure 8. RMS and FFT harmonics of unsteady surface pressure for airfoil gust response at 15, 18 and 19m/s, quasilinear structural model

We now focus on the airfoil post-flutter response with different amplitudes of LCO, and compare the quasilinear and nonlinear structural response models for the highest examined flow velocity of 19m/s. Figs. 7 and 8 first compare results based on Eq. (4). Note a remarkable shift in the frequency and amplitude of the structural response observed for the case of 19m/s. The observed time histories can be roughly subdivided into three periods corresponding to the initial transient development, followed by a period characterized by high amplitude and higher LCO frequency of the unsteady structural and aerodynamic responses, and then the final period with established, lower LCO frequency and amplitude. The LCO frequency shift for 19m/s is clearly observed in the FFT spectra, with two distinct peaks at $\omega_{LCO} \sim 0.6$ and 0.2. Note that the established LCO frequencies are different for the cases of 18 and 19m/s. At the same time, the gust excitation frequency is visible only in the aerodynamic response for 19m/s, with its amplitude now dominated by the structural response. The corresponding unsteady surface pressure fluctuations are shown in Fig. 8 that further demonstrates such dominance. The gust frequency response shows similar amplitudes for all cases, but also reveals an earlier onset of flow instability at 19m/s.

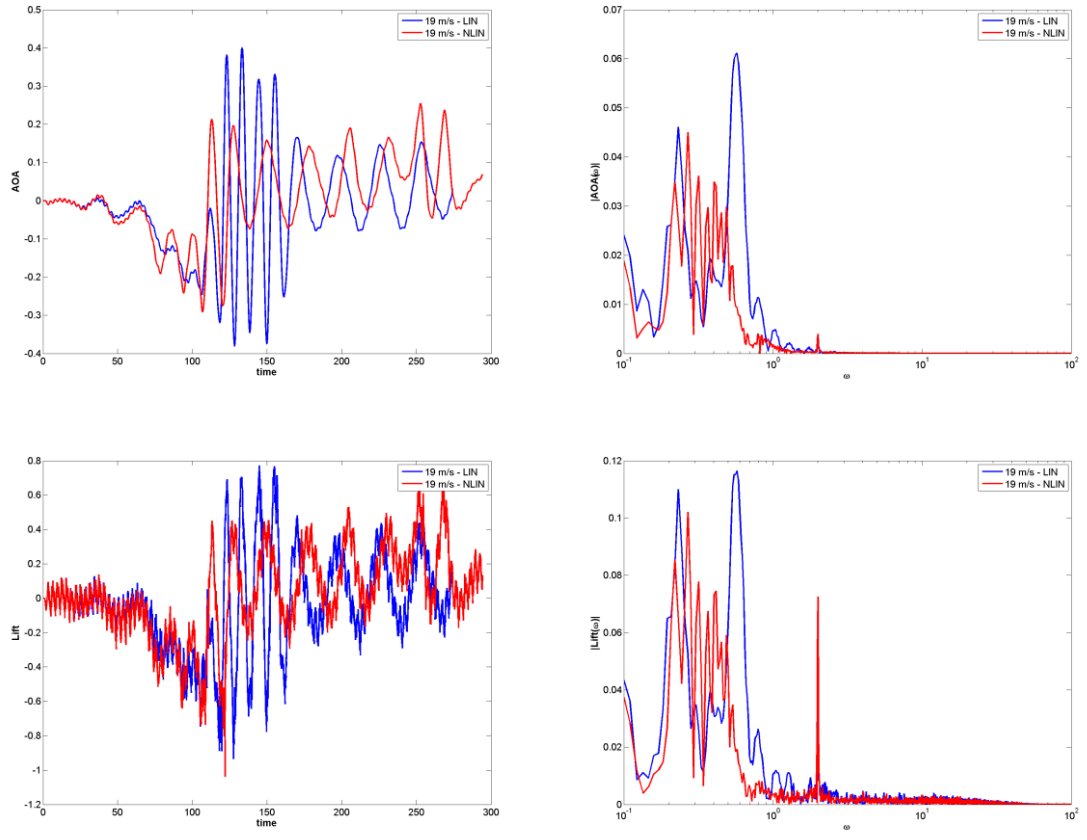

Figure 9. Time histories and FFT spectra for airfoil gust response at 19m/s, quasilinear vs. nonlinear structural models

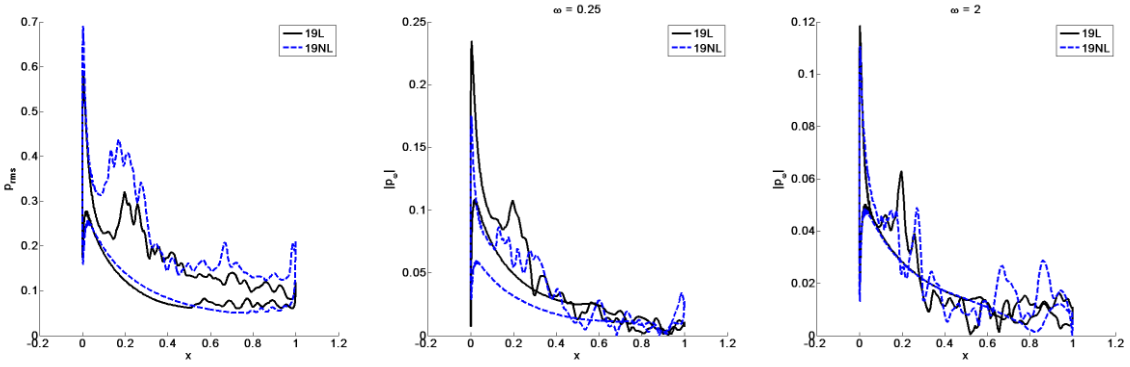

Figure 10. RMS and FFT harmonics of unsteady surface pressure for airfoil gust response at 19m/s, quasilinear vs. nonlinear structural models.

With the amplitudes of pitching and plunging oscillations reaching high values of 23^0 for pitching and 15% of chord for plunging oscillations at 19m/s, the quasilinear structural motion model may not be adequate for such flow regime. To examine the resulting discrepancies, the quasilinear and nonlinear (O'Neil and Strganac, 1998) models are compared in Figs. 9-10. Note that the long-term responses appear similar (except for phase shifts) in Fig. 9 both for LCO frequency and amplitudes. This is also confirmed by good comparison of RMS and harmonics of the unsteady surface pressure in Fig. 10 obtained by processing the last period $\Delta t \approx 50$ of the flow time histories. However, the transient processes observed in Fig. 10 are different, and particularly the high-amplitude oscillations around ω_{LCO} ~ 0.6 are absent in results based on the nonlinear model that rather exhibit a rich spectrum of lower-amplitude transient modes before reaching the final LCOs.

6. CONCLUSIONS

We developed a high-accuracy viscous analysis of strongly coupled nonlinear aerodynamic and aeroelastic unsteady airfoil responses to upstream flow disturbances. In the implemented numerical procedure, Navier-Stokes equations governing the fluid motion were solved simultaneously with equations governing the 2-DOF motion of the structure, so that the fluid and structure were treated as a coupled dynamic system. The numerical procedure employed a high-order low-pass filter operator applied to the dependent variables to selectively damp the poorly resolved high-frequency content and retain numerical accuracy and stability for a wide range of flow operating conditions. For the gust-airfoil interaction study, an efficient model was developed to generate a 2D vortical, incompressible unsteady flow perturbation inside the computational domain through a source term in the momentum equations. The approach conveniently eliminated the need to impose the perturbation at the upstream boundary, which allowed for an efficient grid stretching throughout the far-field to remove any spurious reflections.

The study considered a 1-DOF aeroelastic pitching response of the rigid symmetrical Joukowski airfoil to the 2D gust with the gust reduced frequency k_g =1 and amplitude ε_g =0.1. Results were obtained for a viscous flow with Re=50,000 and velocities 15m/s, 18m/s and 19m/s corresponding to pre-flutter and post-flutter regimes and typical of MAV wing flow conditions. The gust imposed a continuous forced excitation of the structure which responded with oscillations at the gust frequency. The post-flutter regimes showed a distinct superposition of the gust and LCO frequencies, with the latter practically subdued in the case of 15m/s. The comparison of the airfoil surface pressure revealed the unsteady response almost entirely dominated by the gust impact at 15m/s, while above the flutter boundary the effect of the structural motion appeared increasingly more significant. Wide peaks at the LCO frequencies were attributed to the transitional airfoil behavior characterized by frequency shifts towards establishing the long-term structural response. For the highest examined post-flutter flow velocity of 19m/s, the results revealed remarkable LCO frequency and amplitude shifts in the structural response. The comparison of the quasilinear and nonlinear structural response models indicated different transient processes towards establishing similar final LCO patterns with a phase shift. In particular, the quasilinear model revealed a transient region characterized by a high-amplitude LCO at ω_{LCO} ~ 0.6 that abruptly switched to the lower-amplitude LCO at ω_{LCO} ~ 0.2, whereas the nonlinear model reached such long-term response through continuous spectral shift with lower-amplitude transient modes.

Future parametric studies should further elucidate the effects of the gust frequency, amplitude and overall configuration on the coupled unsteady aerodynamic and aeroelastic responses.

7. ACKNOWLEDGEMENTS

The authors are grateful to Dr. Miguel Visbal for support in this work, and to Dr. David Lockard for providing details of 1D gust source modeling.

8. REFERENCES

Anderson, D.A., Tannehill, J.C. and Pletcher, R.H., 1984, "Computational Fluid Mechanics and Heat Transfer," McGraw-Hill Book Company.

Berggren, D., 2004, "Investigation of Limit Cycle Oscillations for a Wing Section with Nonlinear Stiffness," Aerospace Science and Technology, 8, pp. 27-34.

Bisplinghoff, R.L., Ashley, H. and Halfman, R.L., 1957, "Aeroelasticity," Addison-Wesley.

Golubev, V.V., Mankbadi, R.R. and Hixon, R., 2005, "Space-Time Mapping Analysis of Airfoil Nonlinear Interaction with Unsteady Inviscid Flow," AIAA Journal, 43, 10, pp. 2147-2156.

Golubev, V.V., Dreyer, B.D., Visbal, M.R., and Golubev, N.V., 2009, "High-Accuracy Viscous Simulation of Gust Interaction with Stationary and Pitching Wing Sections," AIAA Paper 2009-0011, 47th AIAA Aerospace Sciences Meeting and Exhibit, Orlando, January 2009.

Lele, S.K., 1992, "Compact Finite Difference Schemes with Spectral-like Resolution," Journal of Computational Physics, 103, pp. 16–42.

Lockard, D.P. and Morris, P.J., 1998, "Radiated Noise from Airfoils in Realistic Mean Flows," AIAA Journal, 36, 6, pp. 907-914.

O'Neil, T.O. and Strganac, T.W., 1998, "Aeroelastic Response of a Rigid Wing Supported by Nonlinear Springs," Journal of Aircraft, 35, 4, pp. 616-622.

Shyy, W., Lian, Y, Tang, J., Viieru, D. and Liu, H., 2008, "Aerodynamics of Low Reynolds Number Flyers," Cambridge University Press.

Visbal, M.R. and Gaitonde, D.V., 2002, "On the Use of High-Order Finite-Difference Schemes on Curvilinear and Deforming Meshes," Journal of Computational Physics, 181, pp. 155–185.

Visbal, M.R., Morgan, P.E. and Rizzetta, D.P., 2003, "An Implicit LES Approach Based on High-Order Compact Differencing and Filtering Schemes," AIAA Paper 2003-4098, 16th AIAA CFD Conference, Orlando, June 2003.

9. RESPONSIBILITY NOTICE

The authors are the only responsible for the printed material included in this paper.